

Title: Noninvasive whole-body imaging of phosphatidylethanolamine as a cell death marker using ^{99m}Tc -duramycin during TNF-induced SIRS

Tinneke Delvaeye^{1,2,3}, Leonie wyffels^{4,*}, Steven Deleye⁴, Kelly Lemeire¹, Amanda Gonçalves^{1,2,5}, Elke Decrock³, Steven Staelens⁴, Luc Leybaert^{3,#}, Peter Vandenabeele^{1,2,#}, Dmitri V. Krysko^{6,#,*}

¹VIB Center for Inflammation Research, Technologiepark 927, Zwijnaarde-Ghent 9052, Belgium.

²Department of Biomedical Molecular Biology, Ghent University, Technologiepark 927, Zwijnaarde-Ghent 9052, Belgium.

³Department of Basic Medical Sciences – Physiology group, Ghent University, Ghent 9000, Belgium.

⁴Molecular Imaging Center Antwerp, University of Antwerp, Wilrijk 2610, Belgium.

⁵VIB BioImaging Core, Ghent, Technologiepark 927, Zwijnaarde-Ghent 9052, Belgium.

⁶Department of Basic Medical Sciences – Anatomy and Embryology group, Ghent University, Ghent 9000, Belgium.

#These authors share senior authorship.

***Correspondence:**

Prof. Dr. Dmitri V. Krysko, Address: Department of Basic Medical Sciences, University Hospital Ghent, De Pintelaan 185, 9000 Ghent, Tel: +3293323396, Fax: +3293323809, Email: dmitri.krysko@ugent.be

Prof. Dr. Leonie wyffels, Address: Department of Nuclear Medicine, University Hospital Antwerp, Wilrijkstraat 10, 2650 Edegem, Belgium, Tel: +3238215699, Fax: +3238253308, Email: leonie.wyffels@uza.be

First author (PhD student):

Tinneke Delvaeye, Address: Technologiemark 927, 9052 Zwijnaarde, Tel: +3293313714; Email: tinneke.delvaeye@irc.vib-ugent.be

Word count: 5000

Disclosure:

This work was supported by project grants from UGent Special Research Fund (BOF14/GOA/019 to DVK). Research in the LL group is supported by the Fund for Scientific Research Flanders, Belgium (grant G.0A82.13N), the Interuniversity Attraction Poles Program (grant P7/10), Ghent University (BOF) and the Geneeskundige Stichting Koningin Elisabeth (grant STI.DI2.2017.0004.01). Research in the PV group is supported by Belgian grants (Interuniversity Attraction Poles, IAP 7/32), Flemish grants (Research Foundation Flanders: FWO G.0875.11, FWO G.0973.11, FWO G.0A45.12N, FWO G.0787.13N, FWO G.0E04.16N, FWO G.0C31.14N), Methusalem grant (BOF09/01M00709 and BOF16/MET_V/007), Ghent University grants (MRP, GROUP-ID consortium), a grant from the 'Foundation against Cancer' (2012-188) and grants from VIB. TD was paid by FWO G.0A54.13N to DVK and LL and the Methusalem grant to PV (BOF09/01M00709). Research at Antwerp University was funded by University of Antwerp and its University Hospital, Antwerp, Belgium through a post-doctoral research position for SD, an assistant professor position for Lw and an associate professor position for SS.

Running title: Whole-body imaging during TNF-SIRS

ABSTRACT

Systemic inflammatory response syndrome (SIRS) is an inflammatory state affecting the whole body. It is associated with the presence of pro- and anti-inflammatory cytokines in serum, including tumor necrosis factor (TNF). TNF has multiple effects and leads to cytokine production, leukocyte infiltration, blood pressure reduction and coagulation, thereby contributing to tissue damage and organ failure. A sterile mouse model of sepsis, TNF-induced SIRS, was used to visualize the temporal and spatial distribution of damage in susceptible tissues during SIRS. For this, a radiopharmaceutical agent, ^{99m}Tc -duramycin, binding to exposed phosphatidylethanolamine on dying cells, was longitudinally visualized using single photon emission computed tomography (SPECT/CT) imaging.

Methods: C57Bl/6J mice were challenged with intravenous (i.v.) injections of murine TNF or vehicle, and necrostatin-1 (Nec-1) was used to interfere with cell death. Two h post vehicle- or TNF-treatment, mice received ^{99m}Tc -duramycin i.v. (35.44 ± 3.80 MBq). Static whole-body ^{99m}Tc -duramycin SPECT/CT imaging was performed 2, 4 and 6 h post-tracer injection. Tracer uptake in different organs was quantified by volumes of interest analysis using PMOD software and expressed as mean Standard Uptake Value (SUV_{mean}). After the last scan, *ex vivo* biodistribution was performed to validate the SPECT imaging data. Lastly, terminal deoxynucleotidyl-transferase mediated deoxyuridine triphosphate nick-end labeling (TUNEL) staining was performed to correlate the obtained results to cell death.

Results: An increased ^{99m}Tc -duramycin uptake was detected in mice injected with TNF, when compared to control mice in lungs (0.55 ± 0.05 vs 0.34 ± 0.03), intestine (0.75 ± 0.06 vs 0.56 ± 0.05) and liver (1.03 ± 0.09 vs 0.64 ± 0.02) 4 h post TNF, and remained significantly elevated until 8 h post TNF. The imaging results were consistent with *ex vivo* γ -counting results. Significant increased levels of tissue damage were detected via TUNEL staining in the lungs and intestine of mice injected with

TNF. Interestingly, Nec-1 pretreatment conferred protection against lethal SIRS and reduced the ^{99m}Tc -duramycin-uptake in the lungs, 8 h post TNF (SUV = 0.32 ± 0.04 vs 0.51 ± 0.08).

Conclusion: This study demonstrates that noninvasive ^{99m}Tc -duramycin SPECT imaging can be used to characterize temporal and spatial kinetics of injury and cell death in susceptible tissues during TNF-induced SIRS, making it useful for global, whole-body assessment of tissue damage during diseases associated with inflammation and injury.

Keywords: Necrostatin-1; damage; sepsis; ^{99m}Tc -duramycin; SPECT imaging

INTRODUCTION

Acute systemic inflammation occurs in many severe conditions, such as sepsis, severe burns, hemorrhage and ischemia/reperfusion, and serves to remove invading micro-organisms and to restore homeostasis (1,2). However, an unbalanced and uncontrolled regulation of the inflammatory response causes systemic inflammatory response syndrome (SIRS) (3), which is correlated with a “cytokine storm” in the circulation, i.e. production and secretion of pro-inflammatory cytokines, including tumor necrosis factor (TNF) (4). Subsequently, an amplification in cytokine release, leukocyte infiltration, microvascular dysfunction, consecutive hypotension and coagulation leads to oxygen deprivation in different tissues, which induces cell death and damage in many organs, a state also known as multiple organ injury (5). Various experimental models exist to mimic SIRS *in vivo*, of which in one TNF is injected intravenously (i.v.), thereby mimicking the acute hyper-inflammatory phase of SIRS. TNF-induced SIRS is a well-known commonly used mouse model of sterile sepsis (6-8), which was also used in this study.

Receptor-interacting protein kinases (RIPK), which are implicated in apoptosis, and a regulated form of necrosis, also known as necroptosis (9), were previously reported to play a crucial role in the TNF-induced SIRS pathology (6,8,10). Dead or dying cells, dependent on the cell death modality, manifest different characteristics, going from membrane blebbing in apoptosis, to complete cell disruption in necroptosis. Intriguingly, both apoptotic as well as necroptotic cells display a similar loss of lipid asymmetry in their plasma membranes (PM), by translocation of different phospholipids from the inner PM leaflet to the outer PM leaflet (11). The best-studied ‘flipped’ phospholipids in the context of cell death are phosphatidylserine (12-14) and phosphatidylethanolamine (15,16), which thus represent interesting targets for cell death visualization, during e.g. SIRS, or ischemia/reperfusion. Imaging of phosphatidylserine and phosphatidylethanolamine can be performed through selective binding by Annexin-V (17-19) or duramycin (15,20) respectively, both of which can be bio-conjugated or labeled. As the specificity of

Annexin-V to bind phosphatidylserine disappears in the absence of Ca^{2+} (21), and high abdominal background levels complicate Annexin-based image analysis, the specific binding of the lantibiotic probe duramycin to phosphatidylethanolamine pops up as an attractive alternative. Due to its high affinity to phosphatidylethanolamine, its very stable and rigid character, and because of its lack of cross-reactivity with other phospholipids, it is an easy and specific tool to employ in *in vivo* imaging studies (15,22). Due to the known limitations associated with the use of avidin-biotin systems (background) and green fluorescent protein (poor light penetration through tissues), technetium-99m ($^{99\text{m}}\text{Tc}$) is one of the most widely used radiolabels for duramycin. As such, $^{99\text{m}}\text{Tc}$ -duramycin has been applied extensively to detect dead/dying cells *in vivo*, e.g. in atherosclerotic plaques (23), in tumors challenged to different chemotherapy or radiotherapy schemes (24,25) or in different stages of lung injury (26), where it can be useful in the characterization of new cell death biomarkers.

The aim of this study was to characterize the temporal and spatial kinetics of injury in susceptible tissues during TNF-induced SIRS. Therefore, we followed cell death induction in TNF-injected mice, by $^{99\text{m}}\text{Tc}$ -duramycin using non-invasive single photon emission computed tomography (SPECT) imaging. RIPK1 blocking studies, *ex vivo* biodistribution studies and terminal deoxynucleotidyl-transferase-mediated deoxyuridine triphosphate nick-end labeling (TUNEL) stainings were included to validate the imaging data, and to confirm the specificity of $^{99\text{m}}\text{Tc}$ -duramycin in detecting RIPK1-dependent cell death during SIRS. We found a TNF-induced increase in $^{99\text{m}}\text{Tc}$ -duramycin uptake in the lungs, intestine and liver, and we characterized the lungs as a potential target for RIPK1-mediated cell death. Furthermore, TUNEL images of the lungs confirmed the decrease in the degree of cell death after administration of a RIPK1 kinase inhibitor. Non-invasive imaging of cell death during SIRS could be helpful to screen different pathological sites, or to assess the extent of tissue damage, making it an interesting tool for future clinical studies.

MATERIALS AND METHODS

Mice

Male C57Bl/6J wildtype mice were purchased from Janvier (Le Genest, France). All mice were bred in Specific Pathogen-Free conditions, were used at the age of 8-10 weeks and were housed in air-conditioned, temperature-controlled rooms with 14/10-hour light/dark cycles. Food and water were provided *ad libitum*. All experiments were organized according to institutional, national and European animal regulations. All experiments got approved by the animal ethics committee at Antwerp University (ECD 2015-41) and at Ghent University (ECD 2016-029).

TNF-induced Lethal Shock – Monitoring and Sampling

Necrostatin-1 (Nec-1) (Merck; 480065) was dissolved in dimethylsulfoxide, further diluted in endotoxin-free DPBS (Sigma-Aldrich) and injected i.v. in 200 µl at 6.25 mg/kg, 15 min before i.v. injection of murine TNF (10 µg/20 g) in 200 µl endotoxin-free PBS (pH 6.8). Control mice received an equal amount of DPBS i.v. 15 min before challenge with TNF (indicated as 'Vehicle'). Recombinant mouse TNF was produced in *E. coli* and purified (>95%) in the Protein Service Facility (IRC, Ghent, Belgium), with a biological activity of 4.15×10^9 IU/mg (determined with MTT assay). 2 h after TNF injection, 200 µl purified ^{99m}Tc -duramycin (35.44 ± 3.80 MBq) was i.v. injected. Body temperatures were monitored until 8 h after TNF with an electric thermometer (Model 1; Comark Electronics, Norwich, UK).

Radiolabeling of Duramycin

A kit (kindly provided by Molecular Targeting Technologies, Inc, USA) was used for preparation of ^{99m}Tc -duramycin. 1480 MBq ^{99m}Tc -pertechnetate in 500 µl saline was added to the

kit and it was heated for 20 min at 80°C. The obtained ^{99m}Tc -duramycin was purified using high-performance liquid chromatography (as described previously (25)).

***In Vivo* $\mu\text{SPECT/CT}$ Imaging and *Ex-Vivo* Biodistribution Studies**

2, 4 and 6 h after ^{99m}Tc -duramycin injection, 20-min static whole-body images were acquired, followed by 10 min whole-body high-resolution μCT -scans, using a μSPECT -computed tomography (CT) scanner (VECTor/CT, MILabs, The Netherlands) equipped with a rat multipinhole SPECT collimator. Mice were anesthetized with isoflurane ($\sim 2\%$), while body temperatures were preserved using a heating pad. SPECT images were reconstructed with ordered-subsets expectation maximization (10 iterations, 16 subsets) and a 1.2-mm^3 voxel size. A 20% energy window centered on the 140-keV photopeak was used. Volumes of interest were drawn on the $\mu\text{SPECT-CT}$ images using PMOD software (PMOD Technologies, Switzerland) for intestines, lungs, liver and kidneys. ^{99m}Tc -duramycin uptake was quantified as mean standardized uptake values (SUV_{mean}) using the formula: [average radioactivity concentration (in kBq/cm^3) in the volumes of interest]/[decay corrected amount of injected activity (in kBq)/body weight (g)].

After the last static scan (8 h post-TNF or 6 h post-tracer injection), mice were euthanized by cervical dislocation under isoflurane anesthesia, for *ex-vivo* biodistribution. Blood and different organs/tissues were harvested, rinsed in DPBS, blotted dry, weighed and the radioactivity in the samples was counted by an automatic γ -counter (Wizard2 2480, Perkin Elmer, USA). Uptake of ^{99m}Tc -duramycin was decay corrected and presented as percentage injected dose per gram (%I.D./g).

Immunohistochemistry

Histological samples were collected 6 h after TNF injection and evaluated on paraffin sections. Cell death was identified by TUNEL (TMR *in situ* cell death detection kit; Sigma-Aldrich) and counterstained with DAPI (Thermo Fisher Scientific). Micrographs were acquired using a Zeiss Axioscan Z.1 slide scanner (Carl Zeiss, Jenna, Germany) at 20x magnification, with an ORCA Flash4 camera (Hamamatsu Photonics), and illuminated with a HXP 120V light source. Histological data were analyzed using *Volocity* (PerkinElmer, UK) and *QuPath* (GitHub) softwares.

Statistical Analysis

Statistical analysis was performed with GraphPad Prism software (v.7.0) (USA). One-way ANOVA or two-way repeated measures ANOVA tests were used for multiple comparisons between several groups, followed by a Bonferroni post-test. Significant results are indicated with * for $P < 0.05$; ** for $P < 0.01$; *** for $P < 0.001$ or **** for $P < 0.0001$.

RESULTS

TNF-induced SIRS Leads to Higher *In Vivo* Uptake of ^{99m}Tc -duramycin

As TNF-induced SIRS is an acute model, mimicking a cytokine storm and inducing tissue damage only a few hours after TNF is injected (6), we assessed the *in vivo* uptake of ^{99m}Tc -duramycin 4, 6 and 8 h after TNF treatment. TNF led to a significant increased SUV in different organs, including lungs, liver and intestine, when compared to control mice (Fig. 1A). This increase was detected and maintained at the three time points included in this study. The increased uptake of ^{99m}Tc -duramycin in lungs, liver and intestine in TNF treated animals compared to vehicle treated mice was also visible in the SPECT/CT images, generated at 6 and 8 h after TNF treatment (Figs. 1B-D). The obtained *ex vivo* biodistribution data at 8 h post TNF treatment confirmed the increased uptake in lungs, liver and small intestine, while no significant differences in tracer uptake were detected in the other isolated organs and tissues (Fig. 2). The highest accumulation of radioactivity was detected in the kidneys and is a reflection of the normal tracer clearance (Fig. 2) (25). Of note, a significant increase in ^{99m}Tc -duramycin uptake in the kidneys was observed 8 h ($\text{SUV}_{\text{mean}} = 3.4481 \pm 0.79$) after TNF treatment, when compared to 4 h levels ($\text{SUV}_{\text{mean}} = 3.05913 \pm 0.45$), while for the control animals no change in kidney uptake could be detected (Fig. 1A). Nevertheless, due to the high background levels as a result of tracer clearance, the kidneys were not further analyzed in this study.

Nec-1 Significantly Blocks *In Vivo* ^{99m}Tc -duramycin Uptake in Lungs

It is known that inhibition of the kinase activity of RIPK1 by Nec-1 leads to a complete protection against hypothermia and mortality during TNF-induced SIRS (6). Furthermore, a decrease in the release of cytokines, such as interleukin (IL)-6 and IL-1, and of organ damage

parameters, such as alanine aminotransferase, aspartate aminotransferase or creatine kinase, was observed in the circulation of mice receiving Nec-1 pretreatment upon TNF (6). Therefore, we were interested in the effect of Nec-1 on ^{99m}Tc -duramycin uptake, to validate the occurrence of RIPK1-mediated cell death during TNF-induced SIRS. Interestingly, a decreased uptake of ^{99m}Tc -duramycin was visible in the SPECT/CT images of animals treated with Nec-1, compared to the animals receiving vehicle-pretreatment upon TNF injection (Fig. 3A). However, after image quantification, inhibition of RIPK1 kinase activity only led to a significant decrease of ^{99m}Tc -duramycin uptake in the lungs, 8 h after TNF treatment (Fig. 3B), while no significant differences were observed in any of the other examined organs, i.e. intestine and liver (Supplemental Fig. 1). To confirm the protective effect of Nec-1, rectal body temperatures were monitored at each scanning time point, and verified the better outcome upon Nec-1 pretreatment, already visible 6 h and 8 h after TNF (Supplemental Fig. 2).

The Decreased ^{99m}Tc -duramycin Uptake Observed in Lungs Upon Pretreatment with Nec-1 is Correlated to a Reduction in Cell Death

To validate the reduction in cell death in the lungs upon Nec-1, we subsequently performed *ex vivo* TUNEL staining on lung sections, 6 h after TNF injection, with or without pretreatment with Nec-1. This time point was chosen since TUNEL positivity was previously shown to be present after 6 h of TNF in the liver and intestine (6). A significant increase in the percentage of TUNEL-positive cells was observed in the lungs of mice challenged with TNF, while Nec-1 could significantly protect mice against this increase (Figs. 4A and 4B), suggesting a RIPK1-mediated cell death induction in the lungs. These results were in line with the decreased ^{99m}Tc -duramycin uptake in the lungs of mice pretreated with Nec-1 (Fig. 3). Intriguingly, Nec-1 could also protect against cell death induction in ileum, as quantified by TUNEL staining (Fig. 4A), whereas we did not observe any significant effect

of Nec-1 on ^{99m}Tc -duramycin uptake in the intestine (Supplemental Fig. 1). Similarly to *ex vivo* biodistribution data in large intestine (Fig. 2), no significant increase in cell death induction was visible in colon upon TUNEL quantification (Fig. 4A).

DISCUSSION

Our results illustrate that noninvasive whole-body imaging of cell death during SIRS might be helpful to identify damaged tissues and organs throughout the whole body. In the SPECT imaging study, we were able to pinpoint three different organs at risk during TNF-induced SIRS, namely lungs, small intestine and liver. The increase in ^{99m}Tc -duramycin uptake in these organs was obvious 4 h after TNF injection, and was maintained until the last measurement, 8 h post TNF. *Ex vivo* biodistribution studies using γ -counting confirmed these observations. Next, we identified the lungs as a possible target for RIPK1-mediated cell death, as Nec-1 could significantly reduce ^{99m}Tc -duramycin uptake in the lungs and the amount of dying/dead cells as revealed by TUNEL staining. Altogether, our results demonstrate that ^{99m}Tc -duramycin SPECT imaging can allow temporal and spatial imaging of damage in susceptible organs during TNF-induced SIRS, and potentially during other inflammatory diseases associated with cell death dynamics, making it an attractive tool for future clinical studies.

^{99m}Tc -duramycin has been previously utilized in different *in vivo* studies analyzing cell death occurrence (20,25,27). Here, we apply it to follow damage induction in a sterile mouse model of sepsis. Our data illustrate the susceptibility of three different organs towards cell death induction during TNF-induced SIRS, namely lungs, small intestine and liver (Figs. 1A and 4). During SIRS and septic shock, these organs are indeed known to be vulnerable to increased damage, eventually leading to multiple organ failure (28). Duprez *et al.* demonstrated increases in TUNEL positive cells at the level of ileum and liver during TNF-induced SIRS, which was also confirmed in our study. Furthermore, they analyzed different inflammatory cytokines (IL-6, IL1) and organ damage parameters in circulation, such as aspartate aminotransferase and alanine aminotransferase (liver), creatine kinase (heart & kidney) and lactate dehydrogenase (overall tissue damage) and found increased levels upon TNF injection (6). Additionally, they and others showed the involvement of

RIPK1 in the SIRS pathology (6,8), a kinase known to contribute to apoptosis and a regulated form of necrosis, 'necroptosis'. Therefore, we aimed to examine the contribution of RIPK1-mediated cell death during SIRS, via prophylactic administration of Nec-1, a kinase inhibitor of RIPK1 (6). Interestingly, upon administration of Nec-1, we found a significant decrease in ^{99m}Tc -duramycin uptake in the lungs after TNF injection (Fig. 3B). These data are in line with previous observations, where Nec-1 could significantly protect against remote lung injury, caused by circulating damage-associated molecular patterns and pro-inflammatory mediators, upon necrotic kidney transplants (29). Since Zhao *et al.* characterized parthanatos, a Poly [ADP-ribose] polymerase 1 dependent form of cell death, and necroptosis as the main cell death pathways leading to remote lung injury (29), it is conceivable that also during TNF-induced SIRS, different cell death pathways might contribute to the pathology. Hence, the unchanged levels of ^{99m}Tc -duramycin uptake in the intestine and liver upon Nec-1 administration (Supplemental Fig. 1), could be explained by the presence of other cell death pathways involved. Indeed, in the TNF-induced SIRS pathology, the gut was proven susceptible for apoptosis, by use of caspase-3 knockout mice (6), confirming the notion on the presence of different cell death pathways contributing to TNF-induced SIRS.

An important question remaining in our study is why Nec-1 only affects ^{99m}Tc -duramycin uptake in the lungs, and not in the other organs such as ileum, where it was also able to block cell death, as quantified by TUNEL positivity. One possible explanation in this regard could be the differences between both quantification techniques; during TUNEL analysis, only a few sections are analyzed per organ, whereas the SPECT scanning analysis includes the data obtained on whole organ level. Also, while TUNEL staining is based on detection of DNA fragmentation, ^{99m}Tc -duramycin binds to phosphatidylethanolamine, a phospholipid which is flipped to the outer PM leaflet when cells are dying/dead. Thus, it is conceivable that the different cell death detection setups (*ex vivo* vs *in situ*) might give different results. With regard to TUNEL as a quantification technique for cell death, it is important to mention that we solely applied this method to confirm our

results obtained by ^{99m}Tc -duramycin. In order to distinguish apoptotic from necroptotic susceptible regions, a combination of several techniques should be used to correctly characterize the cell death type (30).

In another model of sepsis, known as cecal ligation and puncture, a near-infrared Annexin-V probe (AV-750) was applied to detect susceptible organs during polymicrobial sepsis (31). Surprisingly, the authors found a significant uptake of AV-750, 24 h after cecal ligation and puncture in lymphatic organs such as the thymus, spleen and liver, of which the latter corresponds to our findings (31). However, it has to be noted that Annexin-V, due to its high abdominal background levels, has less future clinical applicability than duramycin (15). With its low molecular weight, and hence better pharmacokinetic profile, duramycin is correlated to lower background signals (15), however, since its clearance occurs mainly in the kidneys, the detection of renal cell death is challenging and remains a drawback of its use. Nevertheless, since different pathologies are linked to cell death, and *in vivo* imaging with e.g. ^{99m}Tc -Annexin-V was performed in patient studies already (19,32), the use of ^{99m}Tc -duramycin to detect cell death in SIRS remains an attractive alternative to monitor SIRS pathologies and to invest in better treatment guidance.

CONCLUSION

In conclusion, we confirmed that different organs, i.e. lungs, intestine and liver, are susceptible for PE-exposure as a marker of cellular damage during TNF-induced SIRS, as shown by increased ^{99m}Tc -duramycin uptake. Furthermore, our study characterized the lungs as a possible target for RIPK1 mediated cell death and hence demonstrates the relevance of blocking different cell death proteins, e.g. by Nec-1, to help in defining the involved cell death pathways during SIRS. Finally, this study demonstrates the usefulness of ^{99m}Tc -duramycin SPECT imaging for spatial and

temporal visualization of cell death and damage during SIRS, and potentially in other diseases, associated with cell death, inflammation and injury.

ACKNOWLEDGEMENTS

We would like to thank Caroline Berghmans for her technical assistance.

REFERENCES

1. Frangogiannis NG, Smith CW, Entman ML. The inflammatory response in myocardial infarction. *Cardiov Res.* 2002;53:31-47.
2. Akira S, Uematsu S, Takeuchi O. Pathogen recognition and innate immunity. *Cell.* 2006;124:783-801.
3. Davies MG, Hagen P-O. Systemic inflammatory response syndrome. *Br J Surg.* 1997;84:920-935.
4. Tracey KJ, Beutler B, Lowry SF, et al. Shock and tissue injury induced by recombinant human cachectin. *Science.* 1986;234:470-474.
5. Angus DC, van der Poll T. Severe sepsis and septic shock. *N Engl J Med.* 2013;369:840-851.
6. Duprez L, Takahashi N, Van Hauwermeiren F, et al. RIP kinase-dependent necrosis drives lethal systemic inflammatory response syndrome. *Immunity.* 2011;35:908-918.
7. Vanden Berghe T, Demon D, Bogaert P, et al. Simultaneous targeting of IL-1 and IL-18 is required for protection against inflammatory and septic shock. *Am J Respir Crit Care Med.* 2014;189:282-291.

8. Newton K, Dugger DL, Maltzman A, et al. RIPK3 deficiency or catalytically inactive RIPK1 provides greater benefit than MLKL deficiency in mouse models of inflammation and tissue injury. *Cell Death Differ.* 2016;23:1565-1576.

9. Pasparakis M, Vandenabeele P. Necroptosis and its role in inflammation. *Nature.* 2015;517:311-320.

10. Moreno-Gonzalez G, Vandenabeele P, Krysko DV. Necroptosis: a novel cell death modality and its potential relevance for critical care medicine. *Am J Respir Crit Care Med.* 2016;194:415-428.

11. Fadeel B, Xue D. The ins and outs of phospholipid asymmetry in the plasma membrane: roles in health and disease. *Crit Rev Biochem Mol Biol.* 2009;44:264-277.

12. Krysko O, de Ridder L, Cornelissen M. Phosphatidylserine exposure during early primary necrosis (oncosis) in JB6 cells as evidenced by immunogold labeling technique. *Apoptosis.* 2004;9:495-500.

13. Krysko O, Aaes TL, Kagan VE, et al. Necroptotic cell death in anti-cancer therapy. *Immunol Rev.* 2017;280:207-219.

14. Gong YN, Guy C, Olauson H, et al. ESCRT-III acts downstream of MLKL to regulate necroptotic cell death and its consequences. *Cell.* 2017;169:286-300 e216.

15. Elvas F, Stroobants S, Wyffels L. Phosphatidylethanolamine targeting for cell death imaging in early treatment response evaluation and disease diagnosis. *Apoptosis*. 2017;22:971-987.
16. Emoto K, Toyama-Sorimachi N, Karasuyama H, Inoue K, Umeda M. Exposure of phosphatidylethanolamine on the surface of apoptotic cells. *Exp Cell Res*. 1997;232:430-434.
17. Blankenberg FG, Katsikis PD, Tait JF, et al. *In vivo* detection and imaging of phosphatidylserine expression during programmed cell death. *Proc Natl Acad Sci U S A*. 1998;95:6349-6354.
18. Vriens PW, Blankenberg FG, Stoot JH, et al. The use of technetium Tc 99M annexin V for in vivo imaging of apoptosis during cardiac allograft rejection. *J Thorac Cardiovasc Surg*. 1998;116:844-853.
19. Hofstra L, Liem IH, Dumont EA, et al. Visualisation of cell death in vivo in patients with acute myocardial infarction. *The Lancet*. 2000;356:209-212.
20. Audi SH, Jacobs ER, Zhao M, Roerig DL, Haworth ST, Clough AV. In vivo detection of hyperoxia-induced pulmonary endothelial cell death using (99m)Tc-duramycin. *Nucl Med Biol*. 2015;42:46-52.

21. Maffey KG, Keil LB, DeBari VA. The influence of lipid composition and divalent cations on annexin V binding to phospholipid mixtures. *Ann Clin Lab Sci.* 2001;31:85-90.

22. Zhao M, Li Z, Bugenhagen S. ^{99m}Tc-labeled duramycin as a novel phosphatidylethanolamine-binding molecular probe. *J Nucl Med.* 2008;49:1345-1352.

23. Liu Z, Larsen BT, Lerman LO, et al. Detection of atherosclerotic plaques in ApoE-deficient mice using (^{99m})Tc-duramycin. *Nucl Med Biol.* 2016;43:496-505.

24. Elvas F, Vangestel C, Pak K, et al. Early prediction of tumor response to treatment: preclinical validation of ^{99m}Tc-duramycin. *J Nucl Med.* 2016;57:805-811.

25. Elvas F, Vangestel C, Rapic S, et al. Characterization of [^{99m}Tc]duramycin as a SPECT imaging agent for early assessment of tumor apoptosis. *Mol Imaging Biol.* 2015;17:838-847.

26. Clough AV, Audi SH, Haworth ST, Roerig DL. Differential lung uptake of ^{99m}Tc-hexamethylpropyleneamine oxime and ^{99m}Tc-duramycin in the chronic hyperoxia rat model. *J Nucl Med.* 2012;53:1984-1991.

27. Zhang Y, Stevenson GD, Barber C, et al. Imaging of rat cerebral ischemia-reperfusion injury using(^{99m})Tc-labeled duramycin. *Nucl Med Biol.* 2013;40:80-88.

28. Singh S, Evans TW. Organ dysfunction during sepsis. *Intensive Care Med.* 2006;32:349-360.
29. Zhao H, Ning J, Lemaire A, et al. Necroptosis and parthanatos are involved in remote lung injury after receiving ischemic renal allografts in rats. *Kidney Int.* 2015;87:738-748.
30. Vanden Berghe T, Grootjans S, Goossens V, et al. Determination of apoptotic and necrotic cell death in vitro and in vivo. *Methods.* 2013;61:117-129.
31. Zou L, Chen HH, Li D, et al. Imaging lymphoid cell death in vivo during polymicrobial sepsis. *Crit Care Med.* 2015;43:2303-2312.
32. Boersma HH, Kietselaer BLJH, Stolk LML, et al. Past, present and future of Annexin A5 - from protein discovery to clinical applications. *J Nucl Med.* 2005;46:2035-2050.

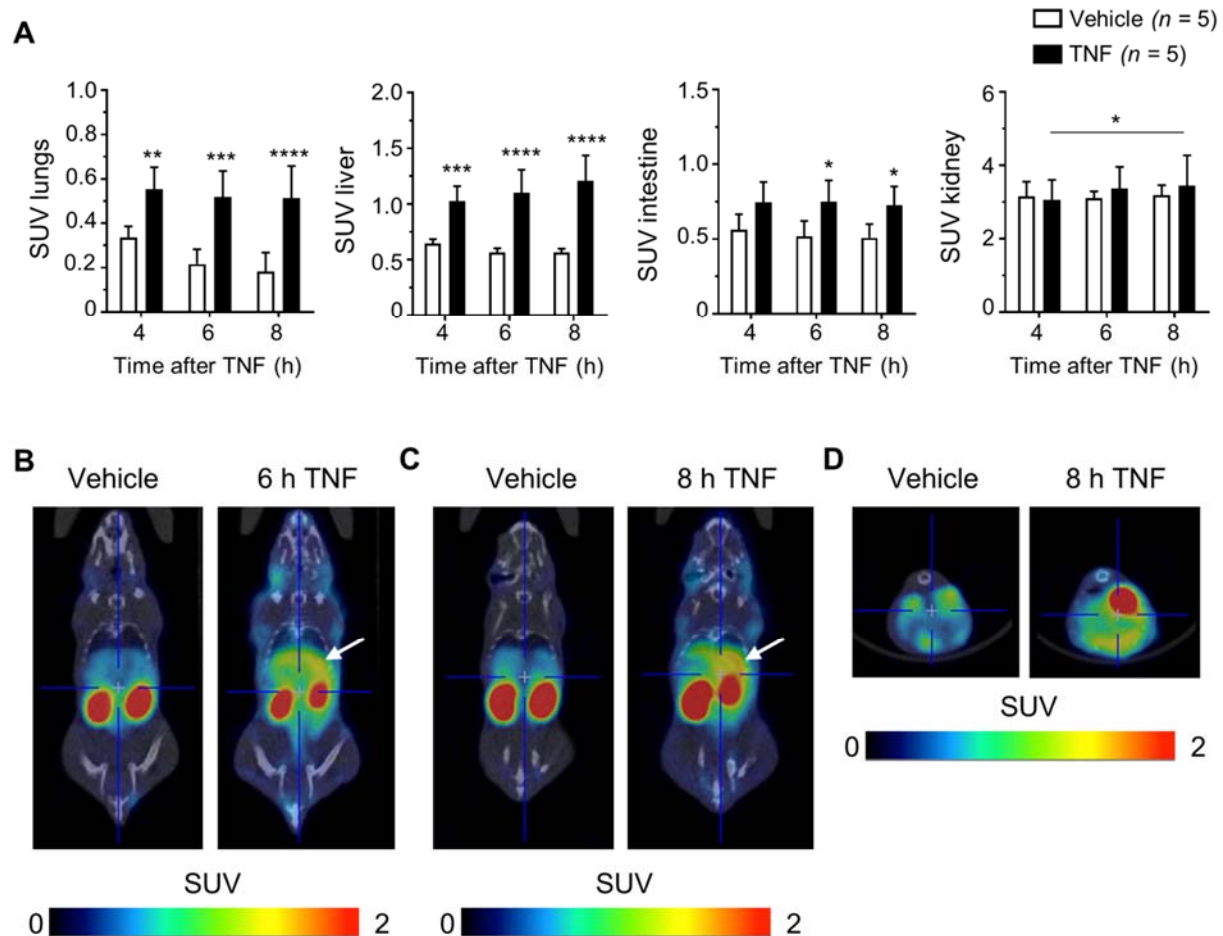


Figure 1: (A) TNF-induced SIRS leads to higher *in vivo* uptake of ^{99m}Tc -duramycin in lungs, liver and intestine 4, 6 and 8 h after TNF treatment. All mice were injected with vehicle (DPBS) or murine TNF (10 μg , i.v.) 2 h prior to i.v. injection of ^{99m}Tc -duramycin (35.44 ± 3.80 MBq). Standard Uptake Values (SUV) are shown at different time points, per organ. Bars represent mean \pm SD of 5 independent experiment days; each day, one animal per group was monitored. n = total number of mice per group. Lungs: **p=0.0058; Intestine (FLTR): *p=0.0137, *p=0.0221; Kidney *p=0.0158; ***p<0.001; ****p<0.0001. **(B-D) Representative coronal SPECT/CT images 6 h (B) or 8 h (C) after vehicle or TNF, and transversal images (D), 8 h after vehicle or TNF.** The regions with higher ^{99m}Tc -duramycin uptake upon TNF treatment, compared to vehicle, are indicated with a white arrow in (B-C).

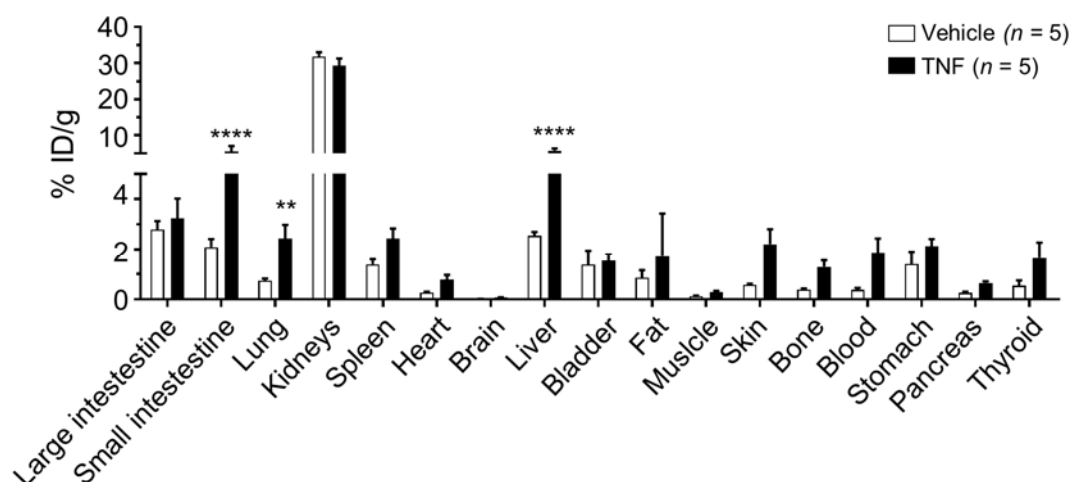


Figure 2: Ex vivo biodistribution of ^{99m}Tc -duramycin in different organs 6 h post-tracer injection and 8 h after TNF. All mice were injected with vehicle (DPBS) or TNF (10 μg , i.v.) 2 h prior to i.v. injection of ^{99m}Tc -duramycin (35.44 ± 3.80 MBq). Uptake levels of ^{99m}Tc -duramycin are presented as percentage injected dose per gram (% I.D./g), 8 h after injection of vehicle or TNF. Bars represent means with SD of 5 independent experiment days; each day, one animal per group was monitored. n = total number of mice per group. The two-star difference corresponds to a p-value of 0.002; ****p<0.0001.

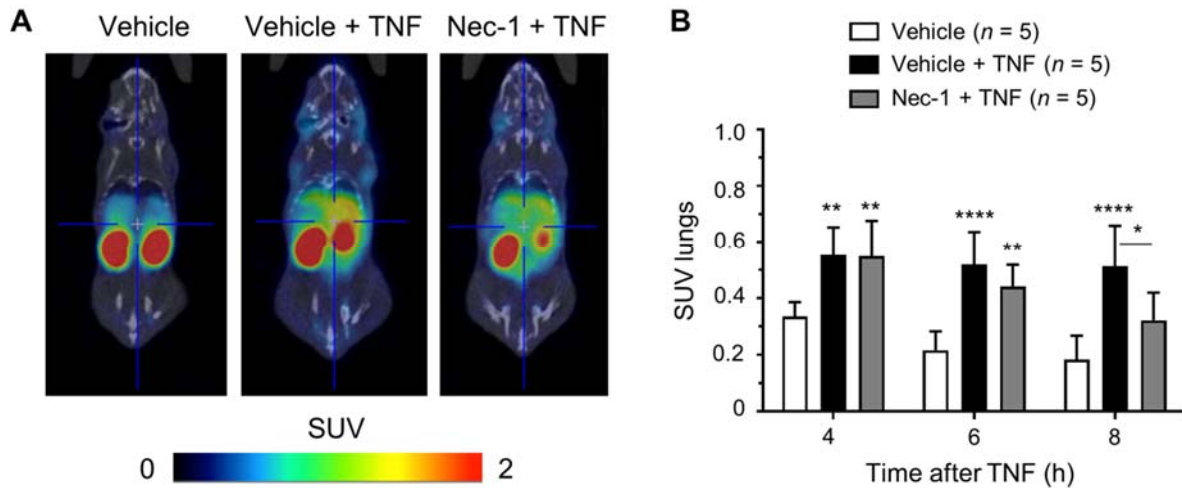


Figure 3: (A) Representative coronal SPECT/CT images 8 h after vehicle, vehicle and TNF or Necrostatin-1 (Nec-1) and TNF. (B) Nec-1 can significantly block *in vivo* uptake of ^{99m}Tc -duramycin in lungs, 8 h after TNF. Male C57Bl/6J wildtype mice were pretreated (i.v.) with vehicle or Nec-1 (6.25 mg/kg), 15 min before injection of TNF (10 μg , i.v.). Mean values with SD pooled from 5 independent experiment days. n = total number of mice per group. The one-star difference corresponds to a p-value of 0.0128; FLTR: **p=0.0041, **p=0.0051, **p=0.0032; ****p<0.0001.

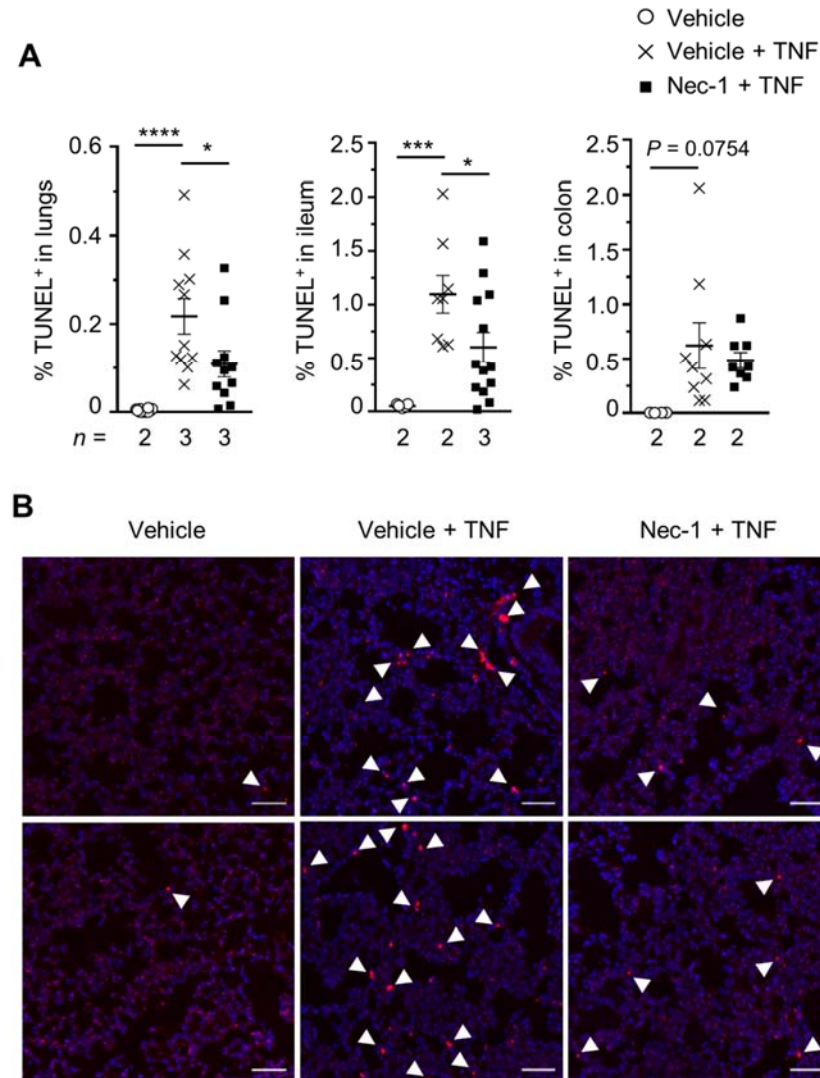
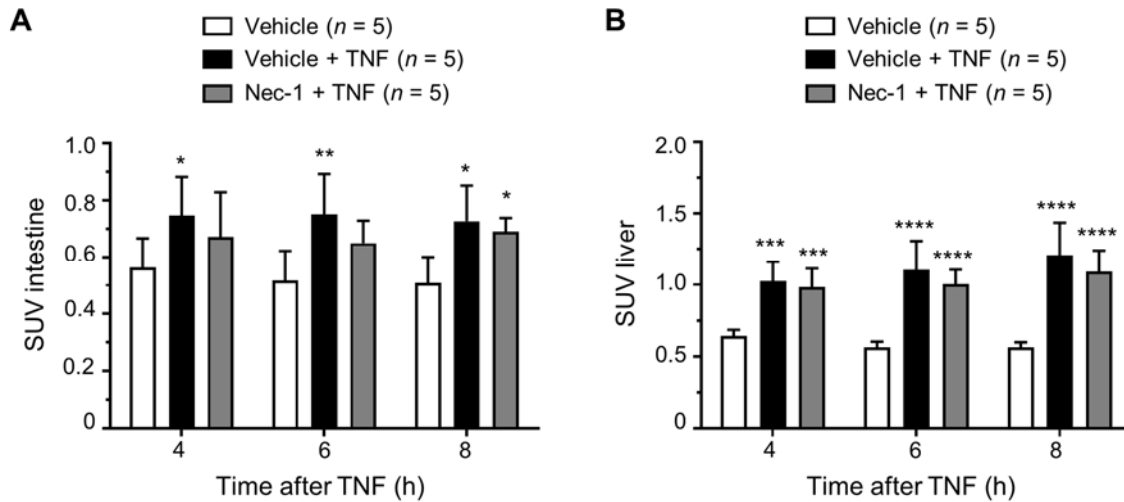
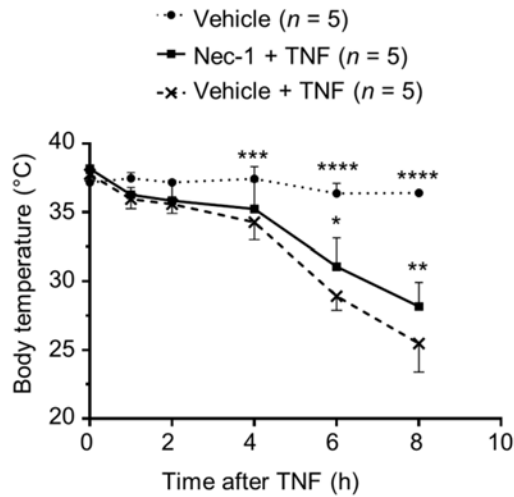


Figure 4: The increase in TUNEL positive cells, observed 6 h after TNF, can be blocked by pretreatment with Nec-1. (A-B) Male C57Bl/6J wildtype mice were pre-injected i.v. with vehicle or Nec-1 (6.25 mg/kg), 15 min before injection of TNF (10 μ g, i.v.). Control mice were injected with vehicle. After 6 h, different organs were isolated and stained for TUNEL positivity. **(A)** Bars represent the ratio of TUNEL positive cells on all cells (DAPI+) (in %). Error bars represent SEM from one experiment. Each individual data point corresponds to one section; n = total number of mice per group; 3-4 sections per organ per mouse. Lungs: *p=0.0369, ****p<0.0001; Ileum: *p=0.0473, ***p<0.001. **(B)** Representative sections of lungs of mice treated with vehicle (left panel; n=2),

vehicle upon TNF (middle panel; n=3), or with Nec-1 upon TNF (right panel; n=3) were analyzed by TUNEL 6 h after TNF. Scale bar = 50 μ m; white arrows indicate TUNEL-positive cells.



Supplemental Figure 1: Necrostatin-1 does not change *in vivo* uptake of ^{99m}Tc -duramycin in intestine (A) and liver (B), at different time-points after TNF treatment. Male C57Bl/6J wildtype mice were pretreated (i.v.) with vehicle or Nec-1 (6.25 mg/kg), 15 min before injection of TNF (10 μg , i.v.). Mean values with SD pooled from 5 independent experiment days. n = total number of mice per group. Stars represent significance towards control (vehicle). Intestine (FLTR): * $p=0.0404$, ** $p=0.007$, * $p=0.0121$, * $p=0.0436$; Liver: *** $p<0.001$, **** $p<0.0001$.



Supplemental Figure 2: Corresponding body temperatures of mice followed in this study.

Male C57BL/6J wildtype mice were pre-injected i.v. with vehicle or Nec-1 15 min prior to injection of TNF (10 μ g, i.v.); n = total number of mice per group. Corresponding body temperatures as a function of time for mice used in Figs 1, 2, 3 and S1. Pool of 5 independent experiment days. Error bars represent SD. The one- and two-star differences have p-values of 0.0119 and 0.0013, respectively; ***p<0.001, ****p<0.0001. Stars represent significance when compared to Vehicle + TNF.



The Journal of
NUCLEAR MEDICINE

Noninvasive whole-body imaging of phosphatidylethanolamine as a cell death marker using ^{99m}Tc -duramycin during TNF-induced SIRS

Tinneke Delvaeye, Leonie wyffels, Steven Deleeye, Kelly Lemeire, Amanda Gonçalves, Elke Decrock, Steven Staelens, Luc Leybaert, Peter Vandenabeele and Dmitri Krysko

J Nucl Med.

Published online: February 1, 2018.

Doi: 10.2967/jnumed.117.205815

This article and updated information are available at:

<http://jnm.snmjournals.org/content/early/2018/01/31/jnumed.117.205815>

Information about reproducing figures, tables, or other portions of this article can be found online at:

<http://jnm.snmjournals.org/site/misc/permission.xhtml>


Information about subscriptions to JNM can be found at:

<http://jnm.snmjournals.org/site/subscriptions/online.xhtml>

JNM ahead of print articles have been peer reviewed and accepted for publication in *JNM*. They have not been copyedited, nor have they appeared in a print or online issue of the journal. Once the accepted manuscripts appear in the *JNM* ahead of print area, they will be prepared for print and online publication, which includes copyediting, typesetting, proofreading, and author review. This process may lead to differences between the accepted version of the manuscript and the final, published version.

The Journal of Nuclear Medicine is published monthly.
SNMMI | Society of Nuclear Medicine and Molecular Imaging
1850 Samuel Morse Drive, Reston, VA 20190.
(Print ISSN: 0161-5505, Online ISSN: 2159-662X)

© Copyright 2018 SNMMI; all rights reserved.

 SOCIETY OF
NUCLEAR MEDICINE
AND MOLECULAR IMAGING